

CHANDRA IMAGING OF THE GAMMA-RAY SOURCE GEV J1809-2327

TIMOTHY M. BRAJE, ROGER W. ROMANI

Department of Physics, Stanford University, Stanford, CA 94305
 timb@astro.stanford.edu, rwr@astro.stanford.edu

MALLORY S.E. ROBERTS

Department of Physics, McGill University, 3600 University St. Montreal, QC. H3A 2T8 Canada
 roberts@hep.physics.mcgill.ca

NOBUYUKI KAWAI

Department of Physics, Tokyo Institute of Technology, Ookayama, Meguro-ku, Tokyo 152-8551, Japan
 and RIKEN, 2-1 Hirosawa, Wako, Saitama 351-0198, Japan

nkawai@tthp1.hp.phys.titech.ac.jp

Draft version October 29, 2018

ABSTRACT

We report on Chandra imaging observations of the Galactic Unidentified γ -ray source GEV J1809-2327, comparing the X-ray images with new VLA 1.46 GHz and 4.86 GHz maps. The X-ray images reveal a point source connected to a non-thermal X-ray/radio nebula, supporting a pulsar/wind model for the γ -ray emitter. We also detect numerous X-ray sources from the young stellar association in the adjacent HII region S32.

Subject headings: gamma rays: observations – pulsars: general – supernova remnants

1. INTRODUCTION

The *EGRET* instrument on the *Compton Gamma Ray Observatory* detected many bright sources along the Galactic plane, most of which remain unidentified. A number of these sources have high significance in $E > \text{GeV}$ photons (Lamb & Macomb 1997), providing relatively good source localizations. The key to making progress on identifications is to search for lower energy, particularly hard X-ray and radio, counterparts. Roberts, Romani, & Kawai (2001, RRK) have carried out an *ASCA* survey of the bright GeV sources to search for counterparts and test the nature of the GeV emitters.

synchrotron wind nebula, or PWN (RRK 2001). This source is also interesting because it is adjacent to the dark cloud Lynds 227 and to the HII region S32 with an embedded association of young high-mass stars. These are plausibly associated with the X-ray source and at $\sim 1.8\text{kpc}$ provide a possible birth site for a pulsar. Oka *et al.* (1999), in a study of the molecular gas in this region, found morphological support for this association and hypothesized that the γ -ray photons were produced when TeV pulsar electrons penetrated the dense molecular gas, suffering relativistic bremsstrahlung losses.

Studies of this complex region were hampered by the modest angular resolution of the *ASCA GIS* ($\sim 3'$ half power diameter), so we have obtained high resolution *ACIS* images to separate out the point source contribution to the X-ray complex. This is abetted by new VLA continuum maps. These data support the pulsar/PWN hypothesis and give new constraints on the origin of the high energy emission.

2. OBSERVATIONS AND DATA ANALYSIS

2.1. CXO Imaging and Source Detection

We observed the gamma-ray source GeV J1809-2327 on 25 August 2000 with the *ACIS* detector (Burke *et al.* 1997) on the Chandra X-Ray Observatory (Weisskopf *et al.* 2000) for $\sim 9.7\text{ks}$. The exposure had the imager chips I0-3 at primary focus with additional off-axis coverage from chips S2 and S3. Integrations were made in TE mode. Basic analysis of the (re-processed) data was accomplished using CIAO v2.2.0.1. We found no evidence of background event rate flares; therefore, the entire dataset was used in the analysis.

Our primary X-ray source list was established using *wavdetect* with a significance threshold of 10^{-7} . Forty four sources are detected with a quoted significance > 3.0 , and in Table 1 we list those sources with a significance of greater than 8.0. The most significant of these are marked in Figure 1. Comparison of our optical and X-ray frames allows us to boresight positions to $\sim 0.3''$. Several of these sources have matches in SIMBAD and the USNO A2 catalogues. Many of these lie in the S32 stellar association to the south of our GeV counterpart

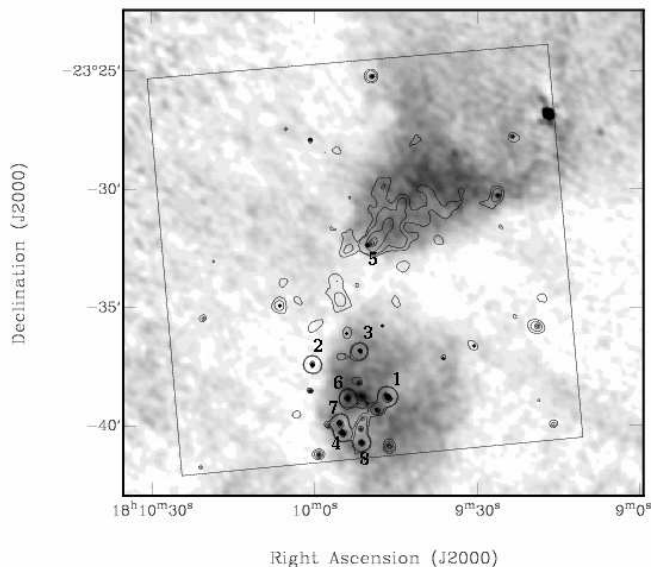


FIG. 1.— VLA 21cm map with *ACIS* 0.5-8keV smoothed contours. The *ACIS*-I FOV (square) and the brightest sources of Table 1 are also indicated.

GeV J1809-2327(=2EG J1811-2339) is one of the brightest, best-localized unidentified plane sources. It is one of a subset of sources showing evidence of γ -ray variability, with an extended hard-spectrum X-ray counterpart argued to be a pulsar

(Figure 1). An overlay of the X-ray image with POSS II scans reveal roughly a dozen additional matches, either with optical $m > 20$ or lower (albeit still high) X-ray significance.

We tested these sources for variability, comparing the individual source photon arrival times to the total image counts (mostly background) arrival times, using the K-S statistic (Press *et al.* 1992). Sources with a variability probability greater than $\sim 95\%$ we regard as likely variables, while most sources are consistent with a constant flux.

As in earlier *ASCA* images, it is evident that in the northern half of the field there is also diffuse X-ray emission. After exposure correction and application of adaptive smoothing filters we find a wedge of diffuse emission in our field with point source 5 at its apex. Figure 1 shows contours from the smoothed image overlaid on a 1.4GHz continuum map. At very low surface brightness below the faintest contours shown, the diffuse X-ray emission seems to extend to the lower left, which might place point source 5 towards the center, rather than apex of the diffuse flux. However, the brightest emission to the NW correlates well with the radio continuum flux.

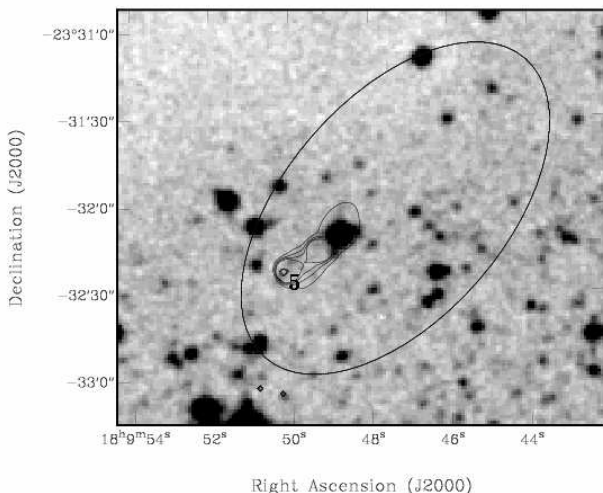


FIG. 2.— DSS image around source 5. Smoothed ACIS contours show the point source and 30'' ‘jet’. The ellipse bounds our nebular extraction region.

Figure 2 overlays X-ray contours on the POSS2 R image. There is no optical point source to the plate limit within $\sim 1.5''$ of the X-ray position. Optical extinction is modest at source 5, but increases rapidly $\sim 30''$ to the NE, toward the edge of Lynds 227. There is significant emission in a narrow jet or trail from point source 5 to the diffuse nebula. In the raw photon counts it shows as a narrow linear feature with a brighter knot $\sim 15''$ from the point source.

2.2. X-ray Spectral Fitting

For the brightest sources ($\gtrsim 80$ counts), we have attempted individual spectral analyses, creating PI spectra, Ancillary Response Files, and Response Matrices. Because of the limited counts and the limited *ACIS* spectral resolution, several spectral models were, in general, formally acceptable. We chose to fit the bright stellar sources in S32 with an absorbed Raymond-Smith plasma model. Fit parameters and multi-dimensional error estimates are listed in Table 1.

2.2.1. Nebula Analysis

Our earlier *ASCA* observations had longer exposure (80ks) and larger effective area. We thus compare present spectral estimates with the higher statistical significance (but spatially unresolved) estimates in RRR. The *ASCA* extraction aperture was quite large (4' radius), so background (particles and Galactic X-rays) dominates the *ACIS* counts in this region. Accordingly, we also define a smaller extraction region (a $68'' \times 38''$ ellipse plus exclusion of the point source) covering the brightest part of the nebula (Fig. 2). In the larger aperture, we attempt to account for the particle-induced background by subtracting the *ACIS* ‘blank-sky’ images. For the smaller aperture, this blank sky subtraction made no significant difference in the source parameters; for this and point source extraction regions, we skip this step. In all cases we carefully chose background regions on the *ACIS-I* chips that were free of obvious emission and spanned a similar range of CCD rows to the source aperture.

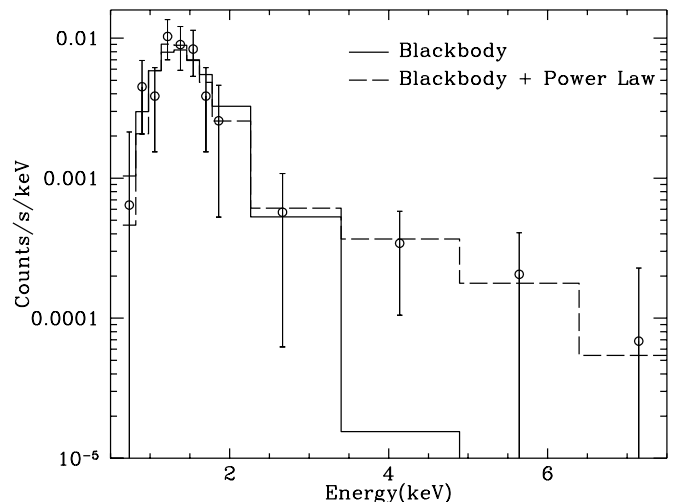


FIG. 3.— Count spectrum and models for point source 5. The excess counts above 3 keV are highly significant and require a hard model component.

ASCA measurements of the diffuse emission determined a power-law index of $\Gamma = 2.09^{+0.18}_{-0.17}$ and an absorption of $N_{\text{H}} = 1.77^{+0.29}_{-0.26} \times 10^{22} \text{cm}^{-2}$ (90% errors). Our fits to the *ACIS* counts in the small extraction region produces values consistent with these (Table 1 – quoted errors are multi-dimensional from the *sherpa* command *projection*). In the larger region we obtain power-law fit parameters several sigma away from the *ASCA* values. We believe that, even with the blank sky subtraction, the dominant particle contribution is not adequately removed in this large aperture. Unlike the small aperture, we also find that the *ACIS* fit parameters are significantly affected by the region chosen for the local background subtraction. If, however, we fix the spectral parameters at the *ASCA*-determined values and fit the counts in the large aperture, we obtain $3.6 \times 10^{-12} \text{erg cm}^{-2} \text{s}^{-1}$ for the *ACIS* data, in good agreement with the flux measured in (RRK 2001). We therefore consider that the *CXO* data are consistent with the *ASCA* fits, but adopt the latter spectral indices as fiducial for the diffuse emission.

2.2.2. Point Source Analysis

For source 5, our counterpart point source, we fit a simple absorbed blackbody. While statistically acceptable, this model cannot produce the counts above 3keV (Figure 3), which

TABLE 1
X-RAY SOURCES

CXOU J Source	Src	Counts	P _{var} (%)	kT (keV)	N _H (10 ²² cm ⁻²)	Flux _{0.5-8.0} (10 ⁻¹⁴ erg cm ⁻² s ⁻¹)	Comments
180926.1-233017	17	30.5 ± 5.9	86.2				
180946.2-234052	12	44.8 ± 7.3	35.1				
180946.6-233846	1	227.1 ± 15.5	96.5	1.07 ^{+0.06} _{-0.08}	0.6 ^{+0.2} _{-0.1}	13 ⁺¹ ₋₁	CD-23 13997 m _V = 9.22, m _B = 9.21
180948.4-233921	13	42.1 ± 7.1	36.5				HD166033 m _V = 8.61, m _B = 8.65
180949.5-232514	9	45.7 ± 7.2	98.8				HD314032 m _V = 9.90, m _B = 10.07
180951.2-234044	8	104.0 ± 10.7	48.7	0.71 ^{+0.13} _{-0.08}	1.3 ^{+0.2} _{-0.2}	4.8 ^{+0.8} _{-0.8}	m _R = 14.5, m _B = 15.1
180951.5-234009	19	38.2 ± 7.1	12.9				
180951.6-233652	3	86.9 ± 9.4	71.6	0.5 ^{+0.1} _{-0.1} (BB)	0.1 ^{+0.3} _{-0.1}	6 ⁺¹ ₋₁	WD 1806-23 m _V = 9.99, m _B = 10.7
180951.8-233811	18	22.3 ± 4.9	11.1				
180953.9-233852	6	110.9 ± 10.8	71.2	0.9 ⁺³ _{-0.3}	1.2 ^{+0.3} _{-0.8}	6.3 ^{+0.9} _{-0.9}	
180954.2-233605	15	19.8 ± 4.5	11.8				
180954.9-234018	4	166.3 ± 13.3	100.0	0.59 ^{+0.09} _{-0.10}	1.2 ^{+0.2} _{-0.1}	7.3 ^{+0.9} _{-0.9}	
180955.4-233954	7	142.7 ± 12.4	57.8	0.9 ⁺² _{-0.1}	1.0 ^{+0.2} _{-0.9}	7.6 ^{+0.9} _{-1.0}	
180957.5-234001	21	26.6 ± 5.6	1.2				
180959.2-234115	10	47.8 ± 7.4	97.8				
181000.4-233726	2	136.3 ± 11.8	98.9	1.0 ^{+0.4} _{-0.1}	1.1 (fixed)	7 ⁺¹ ₋₁	
181000.8-232756	14	21.4 ± 4.7	53.0				
181000.8-233832	16	23.0 ± 4.9	55.9				
181006.4-233456	11	25.6 ± 5.1	48.5				m _R = 15.5, m _B = 17.4
181052.5-233713	20	69.7 ± 11.1	96.5				
nebula	...			Γ = 2.2 ^{+0.4} _{-0.4}	2.2 ^{+0.6} _{-0.5}	59 ⁺⁴ ₋₄	
180950.2-233223	5	85.6 ± 9.3	15.7	0.30 ^{+0.1} _{-0.09} (BB)	0.7 ^{+0.7} _{-0.4}	5.0 ^{+0.8} _{-0.8}	
	5			Γ = 5 ⁺² ₋₁	1.3 ^{+0.9} _{-0.5}	6 ⁺¹ ₋₁	
	5			kT = 0.18 ^{+0.08} _{-0.06} (BB+PL)	1.4 ^{+1.4} _{-0.7}	5 ⁺³ ₋₃ (PL), 3.4 ^{+0.6} _{-0.6} (BB)	

given our small $\sim 2''$ extraction aperture are highly significant (< 0.01 background counts and < 1 pile-up count are expected). Interestingly, several X-ray emitting young pulsars have hard power law components (presumably magnetospheric) superposed on soft thermal spectra (e.g. Saito *et al.* 1997; Halpern & Wang 1997; Pavlov *et al.* 2001), with a typical index $\Gamma = 1.5$. We therefore assume this Γ and fit a powerlaw amplitude from the $E > 3\text{keV}$ source counts. We then fix this power law and re-fit the soft BB component. Parameters for the combined model are listed in Table 1. (with the combined fit smallest by $\sim 2\times$), a result of the low count statistics in the high energy bins.

2.3. Radio Continuum Imaging

Mosaiced continuum observations of the GeV J1809-2327 field at 1.46 GHz and 4.86 GHz were performed with the VLA. Details of the radio observations and full results will be presented elsewhere (Roberts, Gaensler, and Romani in preparation). The 1.46 GHz field (Fig. 1, $18'' \times 15''$ beam) shows diffuse emission associated with S32 and the X-ray PWN; both are also well covered in the 4.86 GHz mosaic.

The S32 region has an inverted, partly thermal spectrum, with spectral index $\alpha \approx 0.1$. The morphology is hollow centered, following the contours of the infrared HII region. In contrast, the wedge of continuum to the north has a non-thermal spectrum, with an approximate spectral index of $\alpha_R \approx -0.3 \pm 0.1$ and significant polarization. The emission follows our diffuse X-ray trail extending $\sim 6'$ to the NW, where the X-ray emission fades below detectability.

3. INTERPRETATION AND CONCLUSIONS

Comparing our new observations with the pulsar+PWN hypothesis, we note that source 5 composite spectrum is characteristic of a young pulsar, with a hard (presumably magneto-

spheric) power law and underlying thermal emission. Given the high $kT = 0.18\text{keV}$, our fit thermal flux implies a small effective area of $A_{\text{eff}} \approx 4 \times 10^{11} (d/1.8\text{kpc})^2 \text{cm}^2$. At $\lesssim 3\%$ of a neutron star's surface, this could represent a polar cap heated by precipitation of magnetospheric particles. Alternatively, atmosphere effects (Romani 1987; Pavlov *et al.* 2001) can produce a hard thermal tail, although such a large fit kT is difficult to produce for reasonable pulsar ages. At a more plausible $kT_{\text{eff}} \lesssim 0.05\text{keV}$, full surface emission from cooling would be unobservable; our data only limit such a component to $< 1.2 \times 10^6 \text{K}$.

Both the power law emission and the hot thermal component can thus measure magnetospheric activity, and have been phenomenologically related to the spin-down luminosity. Becker & Trümper (1997) find that for pulsars observable by ROSAT, the flux scaled as $L_x(0.1-2.4\text{keV}) \approx 10^{-3} \dot{E}$; after correcting for absorption our inferred 0.1-2.4keV flux of $\approx 2 \times 10^{-12} \text{erg cm}^{-2} \text{s}^{-1}$ corresponds to a spin-down luminosity $\dot{E} = 8 \times 10^{35} d_{1.8}^2 \text{erg s}^{-1}$ at the fiducial source distance. Saito *et al.* (1997) find that the (pulsed) ASCA luminosity scales as $L(2-10\text{keV}) \approx 10^{34} \dot{E}_{38}^{3/2} \text{erg s}^{-1}$. Using our 2-10keV unabsorbed point source flux, we infer from this relationship $\dot{E} = 1.5 \times 10^{36} d_{1.8}^{4/3} \text{erg s}^{-1}$. For dipole spindown we have $\dot{E} \approx 10^{38} (B_{12} \tau_4)^{-2} \text{erg s}^{-1}$; these luminosities indicate typical spin parameters for a γ -ray emitting pulsar of $B_{12} \tau_4 \approx 10$, where the surface dipole field is $10^{12} B_{12} \text{G}$ and the pulsar age is $10^4 \tau_4 \text{y}$.

The broadband spectral energy distribution (SED, Figure 4) of our PWN candidate provides some useful constraints on its nature, if we interpret the radio/X-ray spectrum as synchrotron emission from a cooling electron population: $dN_e/d\Gamma_e = A\Gamma_e^{-s}$ with $\Delta s = 1$ at a break Γ_B . This corresponding to a photon break frequency $\nu_B = 4.2 \times 10^{13} B_{10} \Gamma_6^2$, with a typical PWN field of $10 B_{10} \mu\text{G}$ and a electron break at a Lorentz factor $\Gamma_B = 10^6 \Gamma_6$.

Our SED allows a modest range for the power law index $s = 2.85 \pm 0.15$. The data require a very tight correlation between s and the break frequency, $\text{Log}(\nu_B) = 9.1s - 13.3$; however this allows a large range of break energies from the microwave band through the near IR.

The conventional PWN picture identifies this break with the cooling of the electrons at $\tau_4 = 19B_{10}^{-2}\Gamma_6^{-1}$, associating this with the pulsar characteristic age. In this approximation (a homogeneous, uniform field PWN) our data then can be used to eliminate Γ_B in favor of s , giving a PWN field estimate of

$$\text{Log}(B_{10}) \approx 0.73 - 2/3\text{Log}(\tau_4) - 3.03(s-3).$$

The total energy of the electron population, $\approx 10^{47}B_{10}^{(s+1)/2}$ erg, gives an upper limit on the initial pulsar period of $P_i \lesssim 0.4B_{10}^{-(s+1)/4}$ s. Of course, adiabatic losses in the PWN flow likely decrease the present electron energy and require smaller P_i .

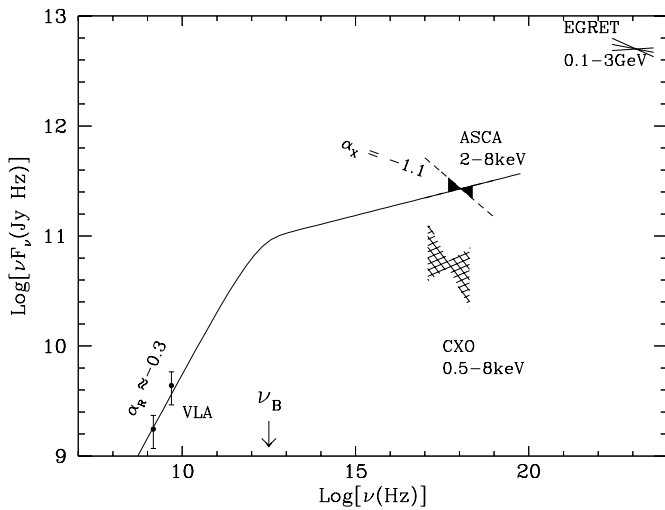


FIG. 4.— Our PWN candidate’s broad-band SED, with X-ray error regions for the full nebula (ASCA) and bright CXO core. The curve is the best-fit $s = 2.85$ cooling synchrotron model.

We can check consistency with another crude estimate of the nebula field. Oka *et al.* (1999) argued that the ‘fit’ of the PWN candidate with Lynds 227 suggests confinement and pressure equilibrium. The CO line-width inferred pressure of $\sim 1.4 \times 10^{-11}$ g/cm/s² implies a nebular equipartition field of $\sim 20\mu\text{G}$. However, since Lynds 227 brackets only on one side, the wind is likely only partly confined and B may be larger. For our best fit s , the equipartition B suggests $\tau_4 \sim 20$, a Geminga-like pulsar. Our present poor constraint on ν_B allows ages $\sim 3 \times 10^4 - 10^6$ y, including $B_{12}\tau_4 \approx 10$ as estimated above. If the PWN B exceeds $20\mu\text{G}$, even smaller τ are permitted.

We can also follow the pulsar surface field B_{12} out to the termination shock in a simple 1-D picture. The magnetic field at $r_s = \theta_s d$, the wind shock radius, is $B_s \sim 3B_* r_*^2 / (r_{LC}^2 r_s) \sim 130(B_{12}\tau_4 d_{1.8}\theta')^{-1}\mu\text{G}$. Beyond r_s the field evolution depends on the poorly understood wind magnetization, but assuming $B_s \approx 20\mu\text{G}$ constant in the postshock wind, for $B_{12}\tau_4 \approx 10$ we expect termination at $\theta_s \approx 40''$. Our ACIS image does not show a spherical wind with a subluminal zone at this θ_s , but instead suggests a jet or pulsar trail, with the $\sim 15''$ knot in the jet/trail plausibly a termination shock. The overall diffuse X-ray morphology suggests a pulsar trail leading back to a PWN, as seen for PSR B1757-24 (Kaspi *et al.* 2001), implying a birthsite to the NW. However, the nebula might also be powered through a jet, as for the asymmetric PSR 1509-58 PWN (c.f. Gaensler *et al.* 2001). In this case the faint extended emission to the SE (Figure 1) may be the counterlobe. Under this interpretation, the S32 cluster at $r \approx 5d_{1.8}\text{pc}$ provides a plausible pulsar birthsite, requiring a pulsar transverse velocity $v_{\perp} \approx 500d_{1.8}/\tau_4$ km/s. Much higher S/N imaging or a proper motion measurement are needed to distinguish these possibilities.

The γ -ray flux is clearly an additional spectral component (Figure 4), but its origin is puzzling. 3EG J1809-2328 (= GeV J1809-2327) is apparently one of the more variable Galactic plane sources (Tompkins 1999). Oka *et al.* (1999) suggested that the PWN-generated electrons penetrate the molecular cloud, generating GeV photons via relativistic Bremsstrahlung. As the PWN is well separated from the molecular gas at $\sim (3')d \sim 1.6\text{pc}$, one might expect variability no faster than the $3l/c \sim 15$ y flow-crossing time. This is substantially longer than the EGRET variability timescale, suggesting an origin closer to the pulsar. Inverse Compton emission from the PWN termination shock seems attractive, but both Galactic IR and local synchrotron emission fluxes fail by several orders of magnitude to account for the required soft photon energy density. Even the optical/UV emission from the OB stars in S32 contribute less than $10^{5.5}L_{\odot}$, failing to produce the required target photon density at the $\sim 5\text{pc}$ PWN distance by $\gtrsim 300\times$. The γ -ray flux is quite plausible for magnetospheric (curvature) pulsar emission at the inferred \dot{E} and distance, but variability is unexpected from an isolated pulsar. Confirmation or exclusion of the γ -ray variability, together with detection or limits on γ -ray pulsations is the best way to address this issue. Unless an X-ray period can be measured, this will not be resolved until AGILE or GLAST make new sensitive γ -ray observations.

This work was supported in part by CXO grant GO0-1125 (RWR) and a Quebec Merit Fellowship (MSER). We thank the referee for a detailed critique.

REFERENCES

- Becker, W. & Trümper J. 1997, A&A 326, 682
 Burke, B.E., Gregory, J., Bautz, M.W., Prigozhin, G.Y., Kissel, S.E., Kosicki, B.N., Loomis, A.H., & Young, D.J. 1997, Transac. Elec. Devices, 44, 1633
 Halpern, J. P. & Wang, F. Y.-H. 1997, ApJ, 477, 905
 Gaensler, B.M., Arons, J., Kaspi, V.M., Pivavaroﬀ, M.J., Kawai, N., & Tamura, K. 2001, ApJ, submitted
 Kaspi, V.M., Gotthelf, E.V., Gaensler, B.M. & Lyutikov, M. 2001, ApJ, in press.
 Lamb, R. C. & Macomb, D. J. 1997, ApJ, 488, 872
 Oka, T., Kawai, N., Naito, T., Horiuchi, T., Namiki, M., Saito, Y., Romani, R. W., & Kifune, T. 1999, ApJ, 526, 764
 Pavlov, G.G., Zavlin, V.E., Sanwal, D., Burwitz, V. & Garmire, G.P. 2001, ApJ, 552, L129
 Press, W. H., Teukolsky, S. A., Vetterling, W. T., & Flannery, B. P. 1992, Numerical Recipes in Fortran, (Cambridge University Press:Cambridge)
 Roberts, M. S. E., Gaensler, & Romani, R. W. 2001, ApJ, (in press)
 Roberts, M.S.E., Romani, R.W., & Kawai, N. 2001, ApJS, 133, 451
 Romani, R.W. 1987, ApJ, 313, 718.
 Saito, Y., Kawai, N., Kamae, T., & Shibata, S. 1997, Neutron Stars and Pulsars: Thirty Years after Discovery, ed. N. Shibazzaki *et al.*, Tokyo, Universal Academy Press, 295
 Tompkins, W. 1999, PhD Thesis, Stanford University
 Weisskopf, M.C., Tananbaum, H.D., Van Speybroeck, L.P., & O’Dell, S.L. 2000, Proc. SPIE, 4012, 2